Journal of Advanced Research 41 (2022) 49–62

Contents lists available at ScienceDirect

Journal of Advanced Research

journal homepage: www.elsevier.com/locate/jare

Original Article

Short range electromagnetic interface using 0.35 μm CMOS blocks for temperature monitoring in isolated areas

Roman Sotner [a,*], Jan Jerabek [b], Ladislav Polak [a], Roman Prokop [c], Umut Engin Ayten [d], Winai Jaikla [e]

[a] Brno University of Technology, Faculty of Electrical Engineering and Communications, Department of Radio Electronics, Technicka 12, 616 00 Brno, Czech Republic
[b] Brno University of Technology, Faculty of Electrical Engineering and Communications, Department of Telecommunications, Technicka 12, 616 00 Brno, Czech Republic
[c] Brno University of Technology, Faculty of Electrical Engineering and Communications, Department of Microelectronics, Technicka 10, 616 00 Brno, Czech Republic
[d] Deptartment of Electronics and Communications Engineering, Yildiz Technical University, Istanbul, Turkey
[e] Department of Engineering Education, School of Industrial Education and Technology, King Mongkut's Institute of Technology Ladkrabang, Bangkog 10520, Thailand

HIGHLIGHTS

- Simple and low-cost system with high immunity against issues of standard optical transmission (vapor, fog).
- Operation without significant path loss of the energy on very short distances for minimization of interferences with other services.
- Bandwidth fitting low-frequency and biomedical applications (from sub-Hz to hundreds of Hz or slowly varying DC voltages).
- Complete implementation of active parts in a form of Application Specific Integrated Circuit for low power consumption and.
- Typical application example in monitoring of environmental features (temperature measurement).

GRAPHICAL ABSTRACT

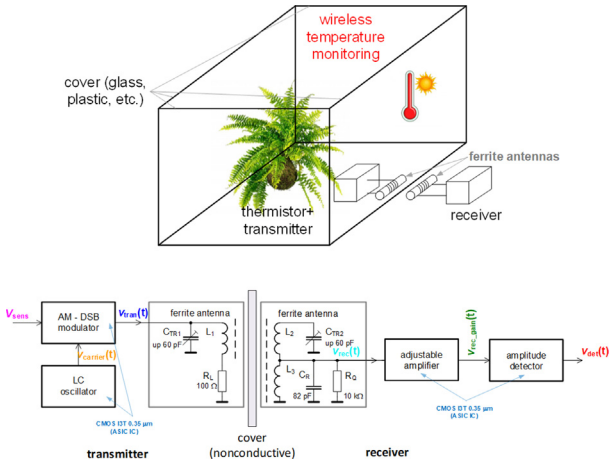

ARTICLE INFO

Article history:
Received 26 October 2021
Revised 22 December 2021
Accepted 10 January 2022
Available online 5 February 2022

Keywords:
Active elements
Amplitude modulation
ASIC
CMOS
Electronic adjustment
Medium radiofrequency wave
Temperature monitoring

ABSTRACT

Introduction: Infra-red (IR) and visible light (VL) based systems developed for transmission of information about physical quantities (e.g. humidity, temperature) out from closed areas, cannot be effectively employed in case of specific conditions in a targeted environment (because of fog or vapor for example).
Objectives: In this work, we introduce a concept of wireless short-range transmitter and receiver to sense physical quantities, for instance temperature, with slow variation. The proposed concept is able to transmit analog-based information from isolated environments (e.g. aquariums or environments for plant growing) with high immunity against vapor and fog that limits standard optical (laser, IR band) methods of communication.
Methods: In this work, a new concept of short range radiofrequency (RF) communication device consisting of transmitting and receiving parts build from active devices fabricated in 0.35 μm I3T25 3.3 V CMOS process and ferrite antennas is selected. RF part uses medium-wave propagation within 10 mm distance at frequency 700 kHz. Such an approach offers minimal path loss of the radiated energy of a signal and low-gain amplification required for restoration of similar levels as available at the transmitting side.
Results: The processing of base-band signals of simple (sine wave) and complex (electrocardiogram)

Peer review under responsibility of Cairo University.
* Corresponding author.
E-mail address: sotner@vut.cz (R. Sotner).

https://doi.org/10.1016/j.jare.2022.01.005

character was verified experimentally through the system. Application example of temperature monitoring in a closed environment, based on a temperature sensor (thermistor), verifies operationability in temperature range from 10 °C up to 50 °C.

Conclusion: Compared to state-of-the-art solution, the presented concept has several advantages, for instance: less complexity; using of simpler type of modulation and demodulation; lower power consumption and significantly reduced issues caused by an environment with special transmission conditions (e.g. fog and vapor). The obtained results are in good agreement with expectations. Among others, the presented system brings beneficial performances for similar applications targeting on monitoring of low-frequency or slowly varying signals.

Introduction

Transmission and distribution of information about physical quantities (humidity, illuminance, temperature, etc.) out from closed areas requiring specific conditions represent key problem of many agriculture environments (plants growing) and aquariums or terrariums [1,2]. Data can be carried in form of optical signal [3–7]. However, this type of communication cannot be used in case of specific conditions in targeted environment (because of fog or vapor for example). In these cases, the optical transmission by the laser or light emitting diode of infra-red (IR) or visible light (VL) [3–7] wavelength is completely useless because it has significant and inestimable attenuation [8–10]. Radiofrequency (RF) communication [11,12] represents a better solution in these specific situations. Majority of works, regarding electromagnetic RF coupling, deals with use of ferrite antennas for energy harvesting purposes [13]. This field is receiving significant attention [14,15]. Especially, the ferrite antennas are used for power transfer in modern automotive technologies [16]. Electromagnetic transmission of information is also important for operation of systems in another specific conditions (e.g. underwater, underground) [17] because electromagnetic wave generated by a magnetic antenna (ferrite) has more effective features for propagation (path loss, size of radiating element) [17] than in the case of dipole antenna (extensive length) at low frequencies. Analog systems for long-wave (LW) and medium-wave (MW) wireless communication (frequencies from hundreds of kHz up to units of MHz) have advantages of simplicity of transmitter (TX), receiver (RX) and antenna system [11,12]. Standard broadcasting systems use very high transmission power for large distance of communication and wide coverage of area by an RF signal [12]. Fortunately, short range operation is possible with significantly lower transmitting powers, losses and requirements on antennas are not high. Advantages of operation with small power, as shown in our case, can be found in almost impossible interference with other services in neighborhood because distances (and ranges of electromagnetic fields) of transmission are very small (tens of centimeter). These cases are sufficiently optimized for near-field distances up to several centimeters. However, it ensures minimal radiation and propagation of sufficient signal level to larger distances than several tens of centimeter (probability of disturbance of further services is insignificant).

Our efforts target on the design of a very simple and effective wireless (electromagnetic) transmission system for distribution of various sensed information on short distance (for instance, 1 cm in tested use case) from isolated areas (aquariums for plant growing purposes, etc.) where other types of communication fail due to specific conditions and behaviors of the environment.

We have compared typical solutions of IR and VL-based system performances with our proposal in Table 1. A simple example (unfortunately targeting on different purpose) of RF system is also included. Illustrational Figure of Merit (FOM) indicates performance of the solution regarding HW/SW complexity and power consumption (where applicable and known). Features included in Table 1 offer the following conclusion:

- many solutions target on digital data transmission [5,6,14], therefore, their performances regarding complexity and costs are quite high,
- many proposed concepts use not so simple [4,7,14] or very demanding special modulation techniques [5,6] requiring extensive circuitry [4,7,14] or advanced signal operations [5,6],
- some solutions require expensive platforms [5,6],
- many concepts are not operating without software [3–6] that increases expenses and complexity of these solutions in comparison to analog concepts,
- structural complexity of some solutions (number of functional blocks) is not low [4–6],
- majority of solutions uses IR or VL-based wireless communication that has not fulfilled requirements on transmission environment with complex features (fog, vapor, etc.) [3–7],
- large transmission distances that can be achieved by the introduced concepts [3,5,6,13] are not necessary because the wireless RF interface is supposed to be placed directly on a nonconductive material forming the border between environments (it helps to minimize possible RF interference because of the minimized transmitting power),
- RF system presented in [13] has different purposes but can be modified (added transmitting part) for our purposes. However, passive solution in [13] requires many modifications including amplification of the received signal and modification of time constants for operation with baseband signals up to several kHz (design in [13] is optimized for DC),
- the most similar concept [14] allows very similar transmission distance, modulation technique and performance, but complexity is extremely large (due to data communication) as well as power consumption and
- the power consumption reaches hundreds of mW or even more (due to complexity and robustness of many systems).

The above listed statements are the motivation for design of a novel system for monitoring of parameters (based on the selected type of sensor and sensed physical quantity) in environments with specific conditions isolated from neighboring areas. Goals and contribution of this work can be summarized as follows:

- design of a simple and low-cost system with high immunity against issues at transmission caused by vapor and fog (where standard optical transmission methods are less effective),
- operation without significant path loss of the energy of the propagated signal and without necessity to amplify very weak signals in far-field region of antennas,
- operationability on very short distances (tens of millimeter) for minimization of interferences with other services,

Table 1
Comparison of similar works in the field using wireless communication or interface for remote sensing of physical quantities from isolated environments.

Reference	Purpose	Type of wireless communication	Transmitted physical quantity (base-band)	Transmission distance (meters)	Modulation technique	Base-band operational bandwidth	Prevailing character of the system	SW not required	Number of blocks	Character of the system (area/topological complexity and processing)	Technology used for design of active devices	Power requirements (maximal used supply voltage / consumption)	For low-cost applications	Transmission not influenced by environmental conditions (humidity, fog, vapor, etc.)	Figure of Merit (FOM)
[3]	medical parameters	IR	time interval	> 1	ON-OFF keying	sub-Hz, Hz	Mixed	No	6	Complex	65 nm CMOS fabricated	1.2 V/ < 7 mW	Yes	No	857
[4]	dimming control	VL + IR	data	N/A	PAM/PWM	N/A	Digital	No	> 8	Complex	N/A	up to 20 W[a]	No	No	0.4
[5]	general data transmission	VL	data	2	OFDM/ PWM	(kbps) kHz	Mixed	No	> 7[b]	Complex	Commercial devices	14 V / 9 W	No	No	0.78
[6]	general data transmission	VL	data	2	OFDM	(Mbps) MHz	Digital	No	> 6	Complex	FPGA, USRP, development board	N/A / N/A	No	No	–
[7]	illuminance measurement	IR	DC voltage	0.2	PWM	kHz	Analog	Yes	6	Simple	180 nm CMOS fabricated	3.3 V / 0.18 W	Yes	No	33
[13]	energy harvesting	RF	various purposes [c]	2500	AM	–	Analog	Yes	3	Simple	passive	–	Yes	Yes	–
[14]	near field measurement (temperature as example)	RF	data	0.02	ASK	(kbps) kHz	Mixed	No	>20	Complex	350 nm CMOS fabricated	3.3 V / 0.27 W	No	Yes	74
Fig. 1	temperature monitoring	RF	DC voltage	0.01	AM	kHz	Analog	Yes	4(5[d])	Simple	350 nm CMOS fabricated	3.3 V / 0.059 W	Yes	Yes	85

Notes: AM – amplitude modulation; ASK – amplitude shift keying; N/A – information not available; BJT – bipolar junction transistor; CMOS – complementary metal oxide semiconductor transistor; VL – visible light, IR – infra red; PAM – pulse amplitude modulation; PWM – pulse width modulation; RF – radiofrequency; DSP – digital signal processor; OFDM – orthogonal frequency division multiplexing; FPGA – field programmable gate array; USRP - Universal Software Radio Peripheral.

[a] – only transmit power (up to 20 W) shown; [b] – complex DSP/microprocessor; [c] – different purpose (broadcasting power 10 kW, received power 62 μW); [d] – including radiofrequency (transmitting and receiving antenna) interface; FOM = number of blocks / overall reported power consumption.

- design of antennas for an RF interface, placed on both sides (opposite each other) of a material (e.g. glass or plastic cover), allowing transmission of sufficient energy for minimal required gain at the receiver side (up to 16 dB) but also minimizing radiation,
- bandwidth of useful signal>1 kHz for low-frequency biomedical applications (from sub-Hz to hundreds of Hz or slowly varying DC voltages),
- complete implementation of active parts in a form of Application Specific Integrated Circuit (ASIC),
- power consumption lower than 100 mW and
- verification of the proposed system in typical application useful for monitoring of environmental features (temperature monitoring in our case).

The contribution of this work is related to the transmission of physical quantities and further information on short distances and it brings design and analysis of a new method using special interface and corresponding counterparts.

The rest of this paper is organized as follows. Section 2 describes the proposed readout of the complete system as well as design and features of partial blocks of the complex scheme. Section 3 targets on the transmission tests and functionality of the complete system. The presented application of remote temperature monitoring is tested in Section 4. Section 5 summarizes the main features of the proposed concept and concludes this paper.

Description of the designed system

The basic principle of the system is shown in Fig. 1. This topology includes a LC oscillator operating at frequency 700 kHz (tunability is possible), a double side band amplitude modulator (AM-DSB) using analog multiplier and a special summing device, two ferrite antennas (for TX and RX), an adjustable amplifier at the side of RX and an active amplitude detector serving as AM demodulator. The used electromagnetic wireless transmission requires operation in long-wave (LW) and medium wave (MW) bands [12]. Therefore, the presented transposition (up-conversion) of the baseband sensed signal to RF band is required. The AM modulation was selected because of simplicity and low requirements on modulation signal. The presented application process DC (slowly changing) voltage where impulse distortion in amplitude of transmitted and received RF signal has insignificant impact (because of filtering and smoothing of modulation signal with long time constant). The sensed signal $v_{sens}(t)$ can be a DC component or slowly changing modulating wave (approximately up to 1 kHz, details are discussed in corresponding subsections). The special analog multiplier with current output terminal [18] provides the product of $v_{sens}(t)$ voltage and carrier wave from LC oscillator and sum of this product with carrier wave (for DSB operation). The resulting wave $v_{tran}(t)$ is then transmitted by a ferrite antenna. The distance between both antennas (distance of coils on ferrite core) was fixed to 10 mm in all performed tests. The receiver of the system includes a tunable antenna optimized for good performance at 700 kHz resonant frequency. The electronically adjustable amplifier using operational transconductance amplifier (OTA) [19,20] provides the amplified voltage $v_{rec}(t)$. Then, the active diode detector using OTA, Schottky diode and voltage buffer demodulates the received waveform back to the baseband or DC signal $v_{det}(t)$. The RF frequency 700 kHz was selected as a compromise between the size of antennas, values of applied tunable elements as well as operational performance of active devices used for construction of system blocks.

LC oscillator

The oscillating circuit uses OTA and grounded passive elements (tunable LC tank as the load including limiting diodes for better stabilizing effects) as shown in Fig. 2. This type of circuit was selected because of the simplicity of the circuit solution best fitting to our requirements. The OTA construction utilizes special multipliers (MLTs) fabricated in I3T25 0.35 μm CMOS process [21]. Detailed information about the MLT performance and CMOS topology is already available in [18], brief principle is a part of Fig. 2. This type of OTA has special feature that the polarity of OTA transfer (direction of output current) can be controlled by the polarity of V_{set_gm} voltage. The transconductance constant, marked a k, required for calculation of transconductance g_m, has value of 1.3 mA/V^2. The characteristic equation of this oscillator has the following form:

$$s^2 + s\frac{(1 - g_{m1}R_o)}{C_{T1}R_o} + \frac{1}{L_{T1}C_{T1}} = 0 \quad (1)$$

where Thomson relation defines oscillation frequency as $\omega_0 = 1/\sqrt{(L_{T1}\cdot C_{T1})}$ and condition of oscillation $g_{m1} \geq 1/R_o$. The resistor R_o represents losses of the LC tank and its major contributing value has output resistance of the OTA ($R_o \cong 100$ kΩ) [18]. The design supposes carrier frequency f_0 = 700 kHz. The selected type of L_{T1} has a value range tunable by ferrite core with screw approximately between 200 and 500 μH. The RF wire-based coil used as an inductor has high frequency performance (tens of MHz), very low DC resistance (units of Ω) and very high value of the quality factor (hundreds). Therefore, real features of the inductor do not influence the performance of the oscillator in the considered bandwidth (f_0 = 700 kHz) and can be neglected. Considering L_{T1} = 500 μH, the theoretically calculated value of C_{T1} yields 103 pF. Real values, used in the design, suppose the existence of parasitic capacitances of printed circuit board (PCB) and nodal parasites of the terminals of MLT and antiparallel diodes ≅ 20–30 pF. Therefore, the real value of C_{T1} must be set by trimmer precisely between 75 and 85 pF. The

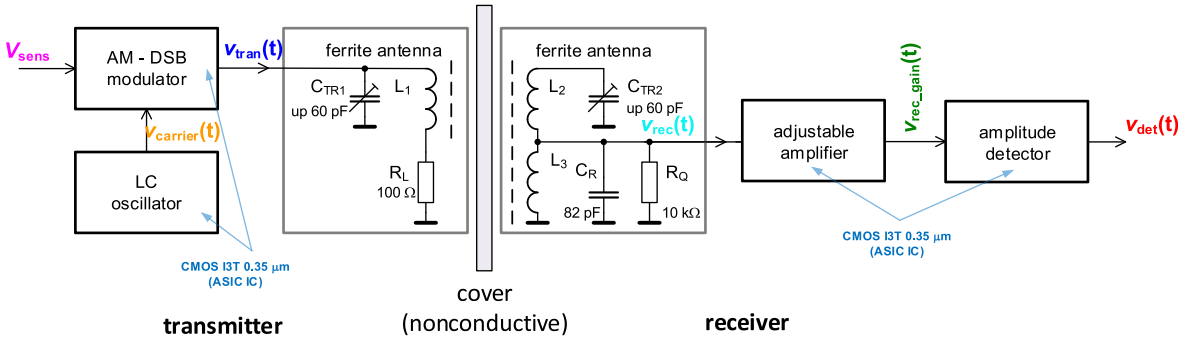

Fig. 1. Complete block concept of proposed transmission system for wireless transfer of sensed voltage value.

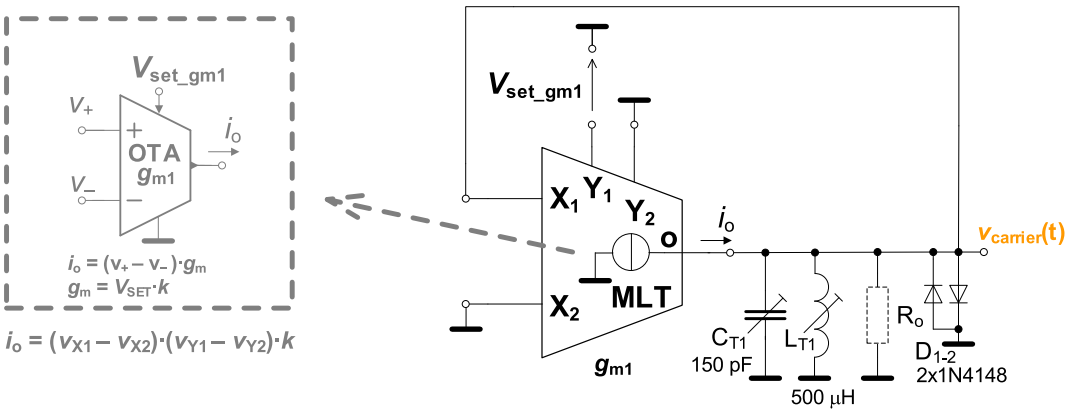

Fig. 2. LC oscillator for modulator (transmitter part).

fulfillment of oscillation condition requires $g_{m1} \geq 10$ μS (V_{set_gm1}- ≥ 7.7 mV, i.e. driving voltage near to 0 V). Results in time and frequency domain are shown in Fig. 3. The produced sine wave has good spectral purity with total harmonic distortion (THD) only around 0.6%. The DSOX-3024 T oscilloscope including integrated generator and frequency response analysis option has been used in the all following experiments.

Temperature variation in the closed environment may have some influences on LC oscillator because the fulfillment of oscillation condition depends on the temperature-dependent g_m of the used OTA. Our design supposes significantly high g_m value ensuring oscillation in any case. The issues with distortion and level variations are solved for fixed frequency (there is no necessity of immediate tunability) by an additional diode limiter applied on the node of LC tank (as shown in Fig. 2). Fig. 3 **(c)** shows simulated

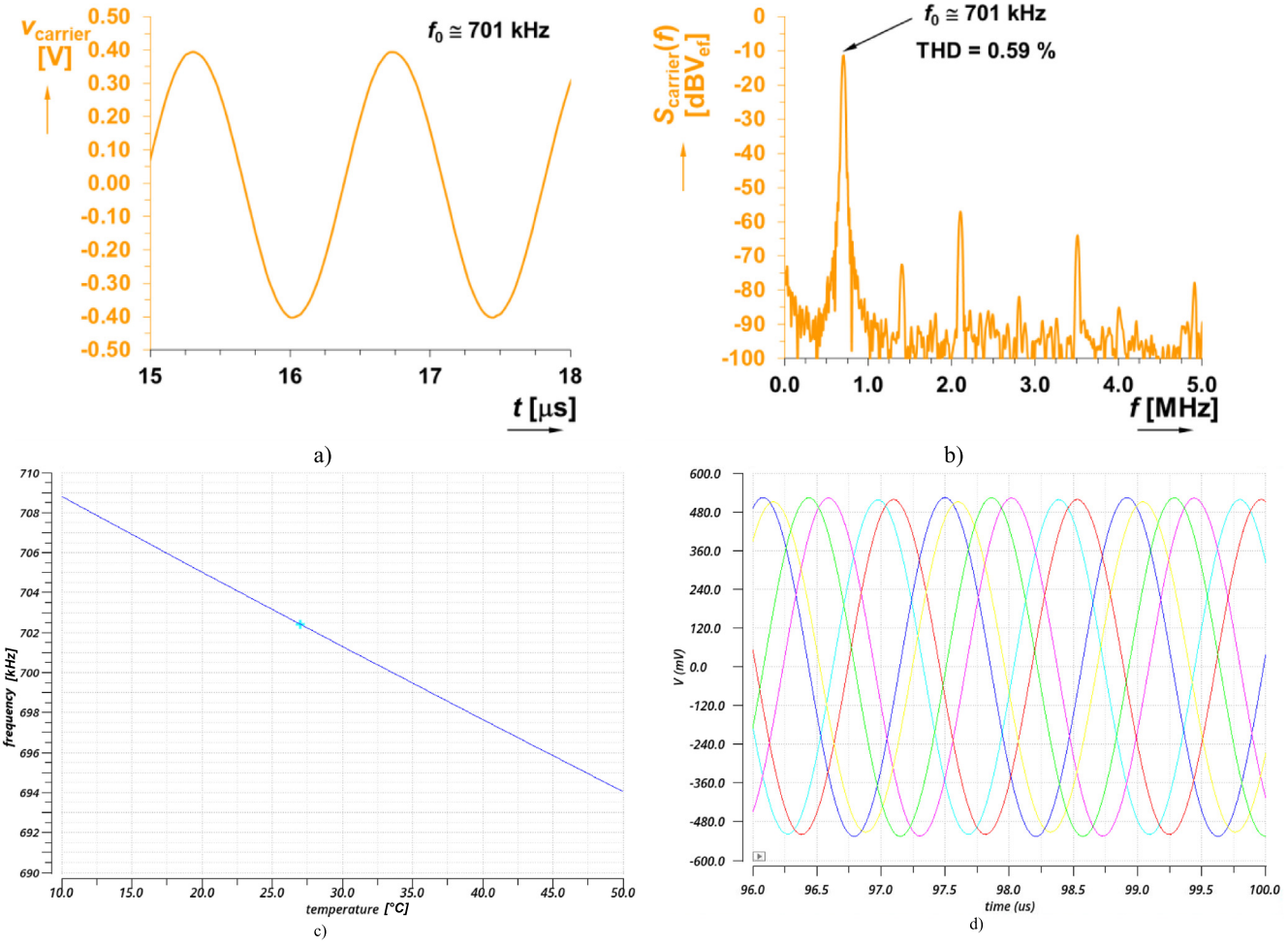

Fig. 3. Experimental test of LC oscillator: a) time domain, b) frequency spectrum, c) Cadence Spectre simulation of dependence of oscillation frequency on temperature, d) example of simulated waveforms of the oscillator during temperature sweep.

(Cadence Spectre using I3T25 process) impact of the temperature (in the observed range) on the accuracy of oscillation frequency (variation between 709 → 694 kHz is insignificant because the transmission path for the modulated wave has bandwidth about 150 kHz). Fig. 3 **(d)** captures almost invariable amplitude level of the oscillator during these simulations. Modeling of inductor (serial resistance in units of Ω and linear temperature coefficient 100 ppm – substantially pessimistic, standard values are in units-tens of ppm) shows that temperature effects influencing LC tank have impact only on certain accuracy of frequency but temperature effects influencing an active device (condition fulfilment) are insignificant due to the used amplitude stabilization.

Double side band amplitude modulator

The AM-DSB amplitude modulator is the key part of the transmitting system. Fig. 4 shows its circuitry using a multiplier (the same as in the previous section) and a so-called voltage differencing differential buffer (VDDB) [18] serving for simple summation of carrier wave with the product of carrier wave and modulation signal (or DC component). The modulation process has the following definition formula:

$$\begin{aligned} v_{tran}(t) &= v_{carrier}(t) + v_{carrier}(t)\cdot v_{sens}(t)\cdot k\cdot R_M \\ &= V_{carrier}[1 + k\cdot R_M\cdot v_{sens}(t)]\cos(\omega_{carrier}t) \end{aligned} \quad (2)$$

The modulation signal $v_{sens}(t) = V_{sens}\cdot\cos(\omega_{sens}\cdot t)$ can be substituted into (2) as:

$$v_{tran}(t) = V_{carrier}[1 + k\cdot R_M\cdot V_{sens}\cos(\omega_{sens}t)]\cos(\omega_{carrier}t) \quad (3)$$

where V_{sens} represents the amplitude of modulating signal or DC component (the cosine part is equal to 1). Experimental verification of the modulator is performed together with the whole system (including RX).

For our purpose, the amplitude modulation (AM) technique was selected as a compromise between simplicity and effectivity of modulator/demodulator. We are monitoring very slowly changing quantity (temperature for example). Therefore, typical issues of AM (e.g. short impulse disturbances in amplitude) are not significant for this application. Moreover, transmission at very short distance between borders of closed environment (section Application example) has significantly high power (attenuation around 7–10 dB) and generates high output levels. Therefore, there is no reason for implementation of another type of modulation scheme.

The VDDB device was used for simplification the operation of summing (it offers better performance than a standard opamp-based summing/subtracting amplifier – no passive elements are required) as well as its availability on fabricated IC (as sub-cells) and suitability to operate as required subparts of the solved systems (this device is used in the case of modulator, amplifier and detector for various purposes – signal operations or as a simple voltage buffer).

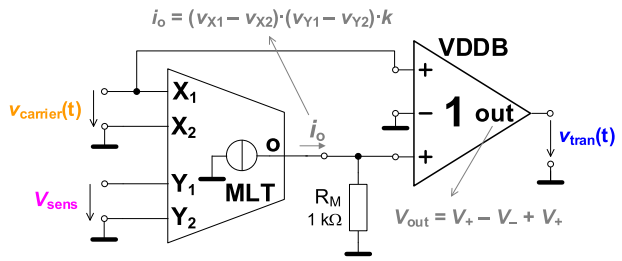

Fig. 4. Double side band amplitude modulator (transmitter part).

Transmitting and receiving ferrite antennas

The ferrite antennas are good choice for the presented use case and transmitting system because of their compact size and weight in comparison with other possibilities in the intended long and medium wave RF bandwidths (several meters long wires, large monopole elements, etc.) [12]. Their low efficiency at the side of TX is not a significant issue for our short-distance purposes [12]. Our wireless interface (see Fig. 5) includes three spirals coiled on two straight rod ferrite cores having circle diameter d = 9 mm and length l = 40 mm. These parameters allow the calculation of the cross-section area of ferrite core $A = \pi\cdot(d/2)^2 = \pi\cdot(9/2)^2 \cong 64$ mm^2. Using nomogram in [12] for initial permeability (first magnetization) of ferrite material μ_i of hundreds and ratio $l/d \cong 4.5$, it yields relative permeability of ferrite rod $\mu_{rod} \cong 23$. Transmitting antenna uses a single spiral L_1. This type of antenna (loop antenna) has a character of resonator and can be approximately considered as an LC resonator. Detailed design procedure is given in [12]. It uses calculation of inductance from Thomson equation expressed for the expected resonant frequency range as: $L_1 = 1/(\omega_r^2\cdot C_{TR1})$. Supposing operation in frequency band around 700 kHz (without any optimization of transmitting antenna for strictly accurate equality $f_r = f_{carrier}$) and trimmer maximal capacity $C_{TR1,2}$ = 60 pF (including parasitic capacity C_p of PCB, interconnection, that means approximately 20–30 pF), the value of L_1 can be estimated from $C_{TR1,2} + C_p$ = 80–90 pF. Then, the value of L_1 will be approximately between 570 and 650 μH and the number of coils results into N = 100–120, based on empiric calculation [12]:

$$N = \sqrt{\frac{l\cdot L}{4\cdot A\cdot \mu_{rod}\cdot 10^{-4}}} \quad (4)$$

The resistor R_L in Fig. 5 presents resistive load of the VDDB device of the modulator (voltage output of the previous stage cannot be directly shorted by inductive load to ground).

The receiving antenna of the RF interface uses two spirals (or inductors) $L_{2,3}$ of very similar inductance values as L_1 (including N). The third spiral L_3 was used for improvement (normally known as a tap between two coils) of voltage transfer in comparison to standard method of impedance separation using only several coils for this tapped output or independent spiral. The capacitor C_R serves for definition (and suppression) of parasitic resonance of the resonator created by L_3 . The resistor R_Q decreases quality factor (avoidance of over-excitation of the following amplifier by the output level of the antenna). These values were set experimentally. Any further impedance matching is not solved because it is insignificant in our case.

Experimental results of this passive part in frequency domain are given in Fig. 6. The real resonant frequency (maximum of transfer) reaches f_r = 676 kHz for C_{TR2} near to maximal value 60 pF

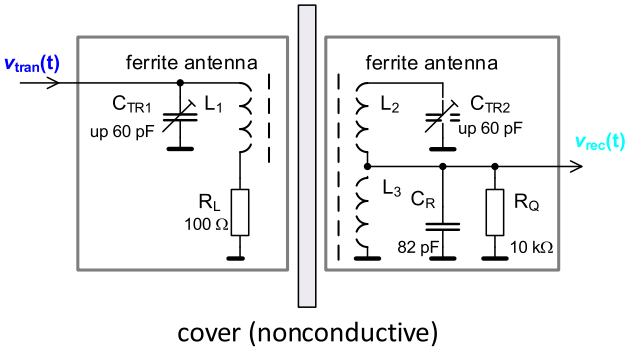

Fig. 5. Wireless RF interface using ferrite antennas.

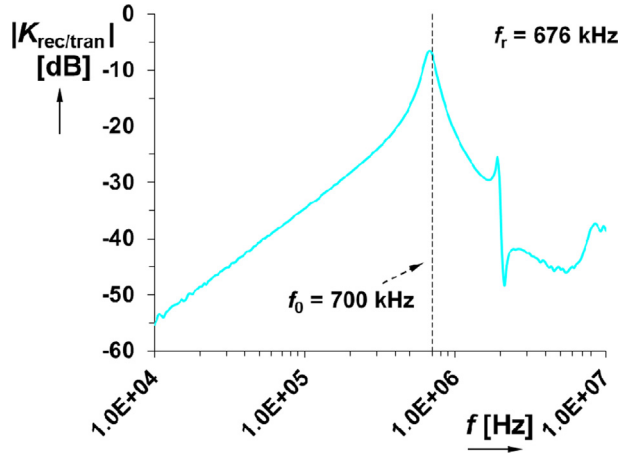

Fig. 6. Frequency response of the designed wireless RF interface.

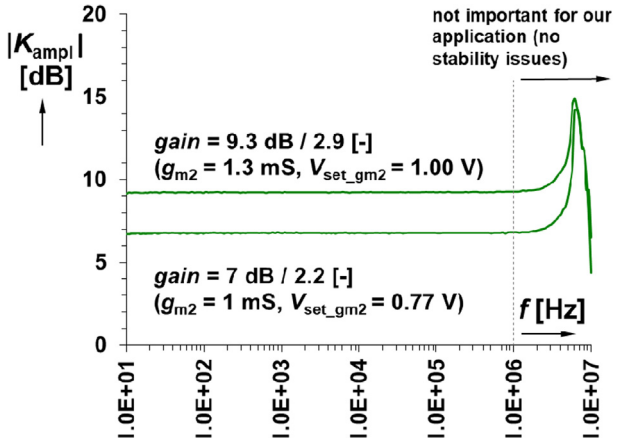

Fig. 8. Example of frequency responses of the amplifier for nominal and maximal adjustable gain.

(around 80 pF including sum of the expected parasites). The maximal gain of this passive interface at frequency f_r yields around – 7 dB. Please note that the difference of operational (700 kHz) and resonant frequency (676 kHz) is insignificant for correct processing. The – 3 dB bandwidth of the RF path yields approximately 150 kHz.

Adjustable amplifier

The multiplier used as an OTA (see Fig. 2) with resistive load R_G and voltage buffer (used for impedance separation – but also applicable without it in our case because detector has high-impedance input) forms the adjustable amplifier (see Fig. 7). Its ideal gain definition has the following form: $K_{ampl} = V_{rec\_gain}/V_{rec} = g_{m2} \cdot R_G$. The maximal available gain for $V_{set\_gm2} = 1$ V ($g_{m2} = 1.3$ mS) reaches approximately 9.3 dB, i.e. 2.9 ($g_{m2} \cdot R_G = 1.3 \cdot 10^{-3} \cdot 2.2 \cdot 10^{3}$). Experimental verification, shown in Fig. 8, indicates a gain of 7 dB, i.e. 2.2, valid for $V_{set\_gm2} = 0.77$ V ($g_{m2} = 1$ mS). This particular value of gain and setting is used to obtain equality of $v_{tran}(t)$ and $v_{rec}(t)$ in further experiments. The presented design considers fitting of features for the expected operational frequency and requirements on sufficient gain. Further gain can be obtained by interconnection of both positive input terminals of VDDB (doubling of voltage) if necessary. The obtained results (amplitude of the tested excitation voltage $V_{rec} = 200$ mV) indicate suitability of available performance for the intended operational bandwidth (carrier frequencies in hundreds of kHz). Peaking in AC response above 5 MHz is given by the response of VDDB [18]. It has insignificant effect and can be further reduced by a proper load of VDDB.

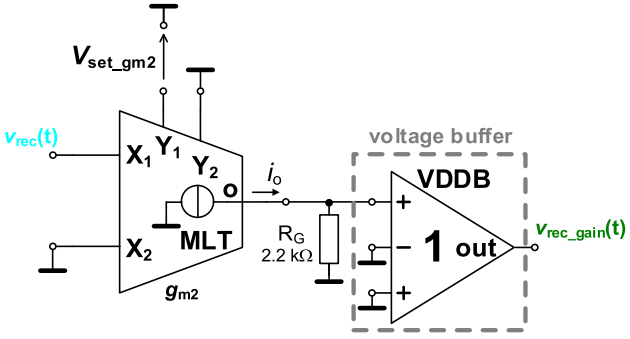

Fig. 7. OTA-based amplifier with resistive load and output voltage buffer (receiver part).

Amplitude detector

The amplitude (peak) detector represents key part for demodulation of AM-DSB signals [11,22]. The newly proposed circuitry uses multiplier and voltage buffer as shown in Fig. 9. An active detector is necessity for low-voltage signals significantly below the threshold of standard silicon diodes. Special Schottky diode BAT42 has been used in our case due to low threshold voltage $V_{th} \cong 0.15$–0.30 V (based on the value of forward current [22]). The AC to DC transfer response can be simply derived. The MLT and VDDB parts (including negative feedback path) form the voltage amplifier providing gain: $G = g_{m3}R_{D1}$ for $v_X(t) \geq V_{th} + v_{det}(t)$. Note that $v_{det}(t)$ has a character of DC component or slowly changing voltage (designed for hundreds of Hz). Then, the output detected voltage can be calculated as:

$$v_{det}(t \text{ or } DC) \cong \frac{G \cdot v_{rec\_gain}(t) - V_{th}}{1 + G} \tag{5}$$

It is clear that gain G influences the value of minimal detectable voltage. In our case, $g_{m3} \cong 3.3$ mS ($V_{set\_gm3} \gg 1.0$ V, dependence of g_m on V_{set_gm} is nonlinear, $k > 1.3$ mA/V^2, then the highest g_m is obtained) and $R_{D1} = 1$ kΩ are used. It yields $G = 3.4$ and, then, $v_{rec\_gain}(t)$ should be larger than approximately 60 mV for $v_{det} \geq 0$ V and $V_{th} = 0.2$ V ($G \cdot v_{rec\_gain} = V_{th}$ for $v_{det} = 0$ V). Note that significant error in this estimation is caused by the exponential dependence of forward current on voltage across diode (considering a threshold value V_{th} is quite inaccurate simplification). This setting also approximately gives the transformation constant (especially for processing of DC signals) of the detector $k_{det} \cong G/(1 + G)$ between the input amplitude and output DC (or slow) voltage. The time constant ($R_{D2} = 10$ kΩ, $C_D = 47$ nF, i.e. $\tau = R_{D2} \cdot C_D \cong 0.5$ ms) was set in order to process modulation signals up to hundreds of Hz correctly. Transfer characteristic and time-domain example are given in Fig. 10.

Test of transmission operationability

The complete block concept shown in Fig. 1 (i.e. all previously discussed circuits interconnected) was experimentally tested for an RF signal path as well as several cases of modulation signal applied to the node V_{sens}. Please note that these results cannot be obtained reliably by simulations due to presence of parts having unavailable model (ferrite antennas of specific design). The first example is the sine wave of amplitude $V_{sens} = 100$ mV and having frequency $f_{sens} = 100$ Hz. The examples of time-domain waveforms through the system are shown in Fig. 11. The input signal $v_{sens}(t)$

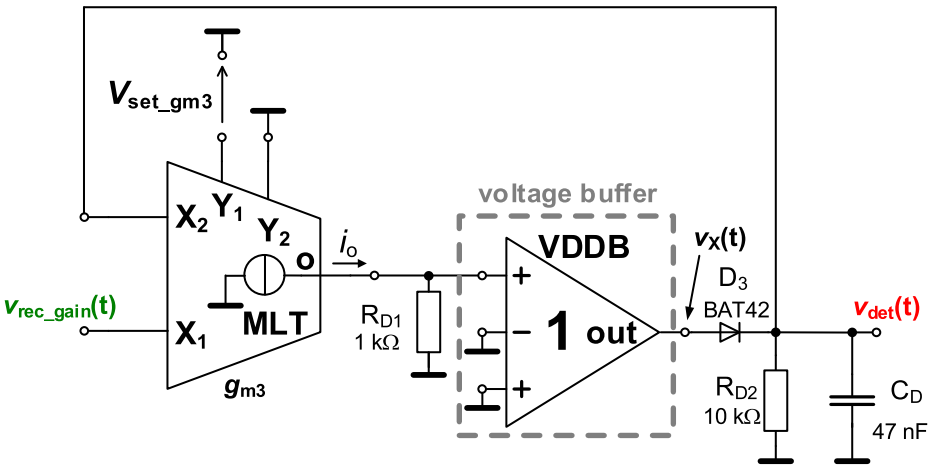

Fig. 9. Active peak detector for simple amplitude demodulation (receiver part).

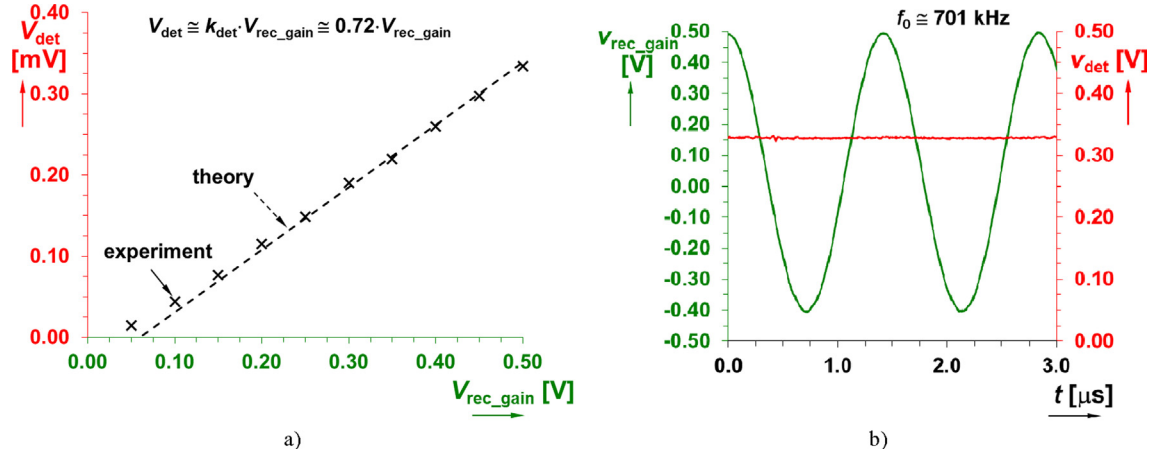

Fig. 10. Analysis of rectifier/detector: a) transfer characteristic between $v_{rec\_gain}(t)$ and v_{det}, b) time-domain example of detection for amplitude V_{rec_gain} = 500 mV.

(violet) and the transmitted signal $v_{tran}(t)$ (blue) are shown in Fig. 11 **(a)** while Fig. 11 **(b)** illustrates the received wave (after amplification) $v_{rec\_gain}(t)$ (green) and the detected (demodulated) modulation signal $v_{det}(t)$ (red). Note that Fig. 11 **(b)** documents $v_{det}(t)$ signal without DC component (AC coupling is used). Frequency spectrum of $v_{det}(t)$ in Fig. 11 **(c)** reports total harmonic distortion THD = 0.34%. Fig. 12 presents AC frequency response of the RF part (between $v_{tran}(t)$, $v_{rec}(t)$ and $v_{rec\_gain}(t)$ respectively) for the following conditions. The blue dashed trace represents transfer response of the antenna itself (identical to Fig. 6). The solid green trace indicates frequency response after adjustable amplifier. The setting of amplifier (Fig. 7) compensates losses of transmission in RF band (700 kHz) caused by ferrite antenna. Its V_{set_gm2} = 0.77 V (g_{m2} = 1 mS) shifts the maximum of gain to $|K_{ampl}|$ = 2.2 (7 dB). It results into the same level of the transmitted and received (after amplification) waveform. The green dashed curve presents response for maximal available gain. These results correspond with time-domain analysis (blue and green signals) shown in Fig. 11.

We also studied the AC transfer of useful $v_{sens}(t)$ (modulation) sine wave signal through the system. Fig. 13 shows the characteristic of transmission channel. It represents low-frequency low pass circuit for the above described nominal setting (RF transfer response without losses between the TX and RX part, i.e. $v_{tran}(t) = v_{rec\_gain}(t)$). The output voltage $v_{det}(t)$ is attenuated by 8 dB in frequency range of interest (i.e. up to $f_{sens} \approx 4$ kHz). Further gain can be obtained by additional low-frequency (bandwidth of several kHz) amplifier or by further amplification of the signal in the RF path avoiding issues with clipping or another effects of nonlinearities on waveforms (overexciting above several hundreds of mV), if necessary.

The system can be used also for transmission of more complex waveforms. The electrocardiogram wave with fast (unreal) repeating frequency 100 Hz was selected as an example of base-band channel performance in order to prove workability in the same frequency range as in Fig. 11 but with non-harmonic signal. The example is captured in Fig. 14 (input $v_{sens}(t)$ and output $v_{det}(t)$ waveforms).

Application example – Temperature monitoring

Information about temperature belongs to a group of very important parameters of environment. The proposed system is able to transmit such information (through electromagnetic field) from a closed environment covered by a nonconductive material as shown for example in Fig. 15 **(a)**. Fig. 15 **(b)** explains a simple circuit producing DC voltage V_{sens} dependent on the resistance of thermistor Epcos NTC-K45-1.0 [24] (with nominal value 1 kΩ) having negative temperature coefficient. The output of this circuit is directly connected to the modulator (see Fig. 1) of transmitting

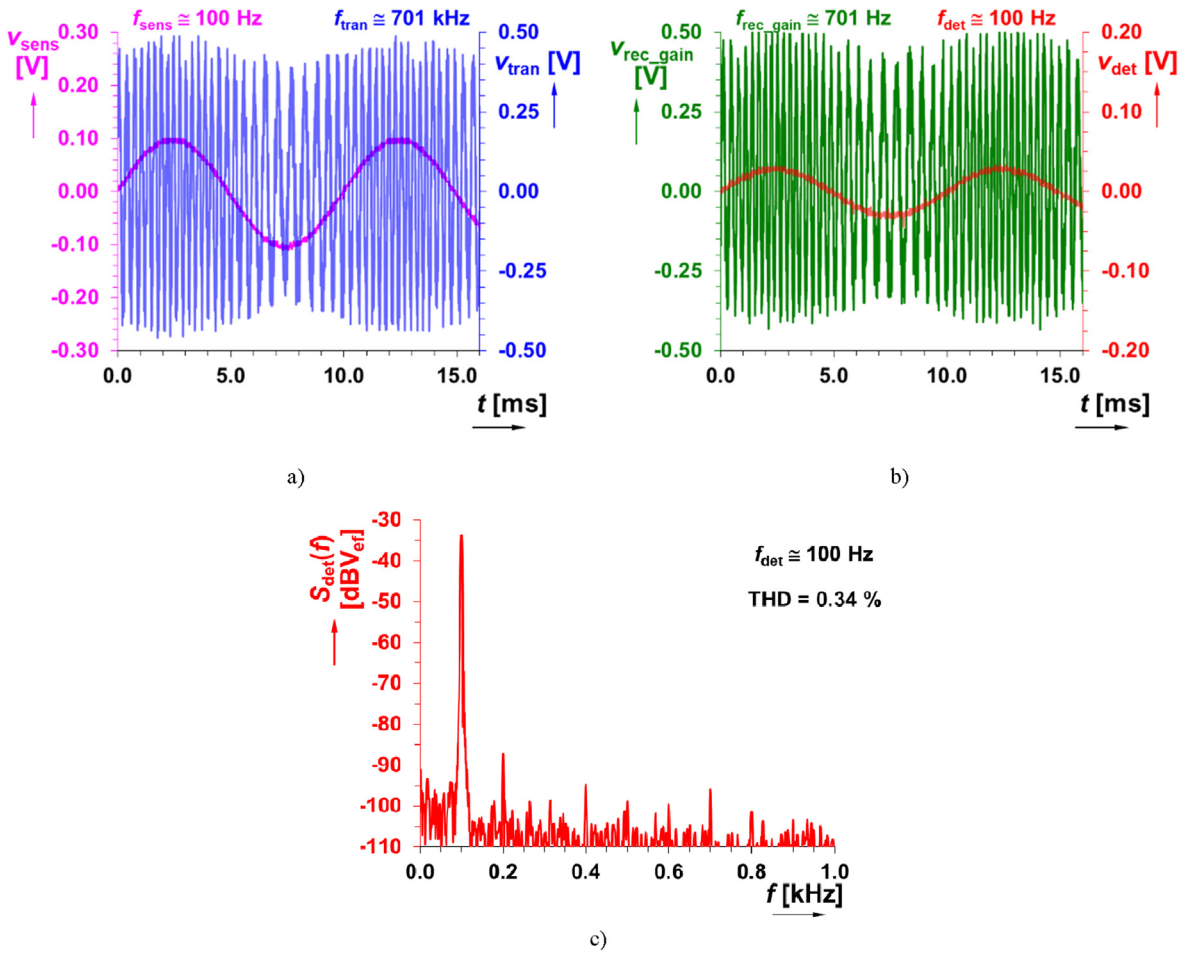

Fig. 11. Time domain responses through important parts of the transmitting and receiving system: a) transmitting side, b) receiving side, c) spectral analysis of demodulated wave $v_{det}(t)$.

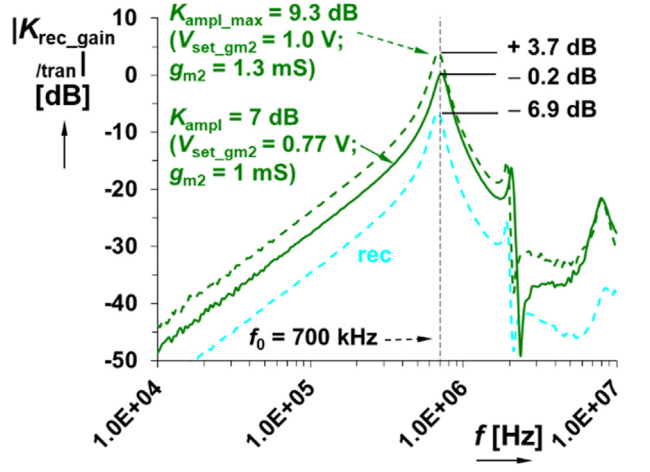

Fig. 12. Frequency response of the transfer through the RF system ($v_{tran}(t) \rightarrow v_{rec\_gain}(t)$).

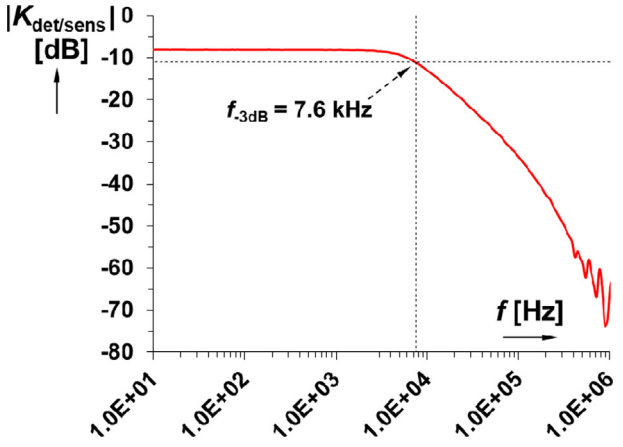

Fig. 13. Frequency response of modulation signal ($v_{sens}(t) \rightarrow v_{det}(t)$) through the system (transfer of low-frequency sine-wave signal is expected).

system. Based on the used thermistor, the targeted range of operation is from 10 °C up to 50 °C. It is sufficient for proving the operation of the proposed transmission system.

The thermistor having negative temperature coefficient (NTC) decreases its value with increasing thermodynamic temperature (T [K] = *temp.* [°C] + 273) in accordance with the following relation [25,26]:

$$R_{NTC}(T) = R_{NTC}(T_0)\exp\left[B_{T_0/T}\left(\frac{1}{T}-\frac{1}{T_0}\right)\right] \quad (6)$$

where nonlinear dependence of resistance of thermistor $R_{NTC}(T)$ on temperature is approximated by exponential function (actually

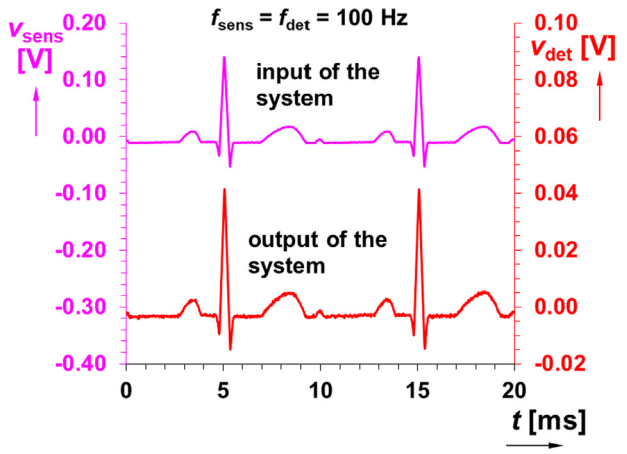

Fig. 14. Example of transmission of more complex signal: input and output signal in time domain (electrocardiogram).

quite inaccurately). Parameter $R_{NTC}(T_0) = 1\ k\Omega$ represents resistivity at ambient temperature T_0 (T_0 = 298 K, *temp.* = 25 °C) and $B_{T0/T} = 3.73$ [kΩ] is called temperature constant approximately valid in limited range given by the manufacturer of this element [24,25]. We tested the temperature monitoring in a range from 9 °C up to 52 °C. This scale of temperatures covers ranges of standard conditions in environments allowing safe and effective plant growing, for example. Moreover, different range or scale (within similar behavior) can be set by appropriate selection of the value of R_S or similar modification of the divider as well as by consideration of larger range of V_{sens}. However, the nonlinear dependence of R_{NTC} on temperature starts to be very significant and nonlinearity error (measurement vs expectation) is more important as well as limitation of dynamics of active elements. The thermistor takes a part of the trivial resistive divider (see Fig. 15 **(b)**) having transfer $k_d = R_{NTC}/(R_{NTC} + R_S)$. It gives DC value of $V_{sens} = 2 \cdot V_{DD} \cdot k_d - V_{SS} = 3.3 \cdot k_d - 1.65$ [V]. Variation of temperature causes change of the value of R_{NTC} as well as transfer k_d and therefore also the value of V_{sens}. Fig. 16 **(a)** illustrates comparison of the expected theoretical trace and experimentally obtained results (real R_{NTC} is calculated from the measured values of V_{sens}). Dependence of generated DC voltage V_{sens} on temperature is captured in Fig. 16 **(b)**. Supposing compensated losses of RF path ($|K_{antenna}| + |K_{ampl}| = 1$), the transfer of voltage through the system has the following approximate expression:

$$V_{det} \cong k_{det} V_{carrier}(1 + V_{sens}) = k_{det} V_{carrier}\left[1 + 2V_{DD}\left(\frac{R_{NTC}(T)}{R_{NTC}(T) + R_S}\right) - V_{SS}\right] \quad (7)$$

in which (6) is substituted to obtain direct relation between temperature and DC output voltage V_{det}. The sensing voltage V_{sens} is transformed by the system to the output voltage V_{det}. Fig. 17 depicts the transforming relation between these voltages. The invariable value of amplitude $V_{carrier}$ = 0.380 V and $k_{det} \cong 0.725$ results into

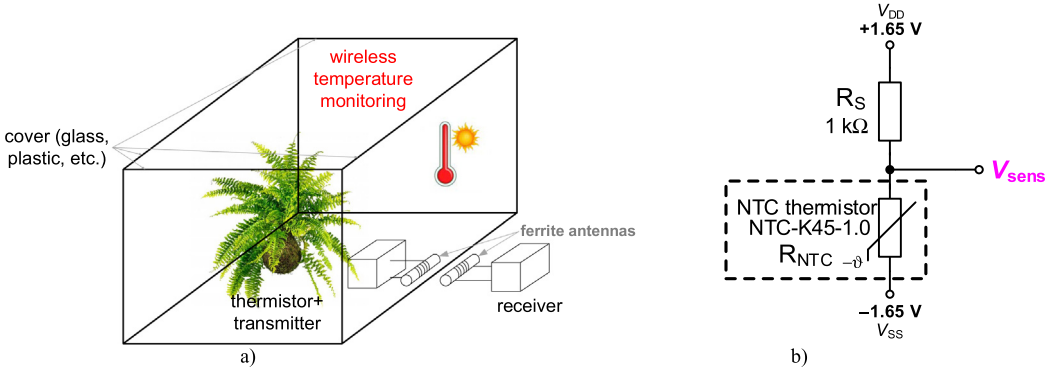

Fig. 15. Temperature monitoring and its wireless transfer out of closed environment: a) illustration of application, b) simple sensing circuit using thermistor.

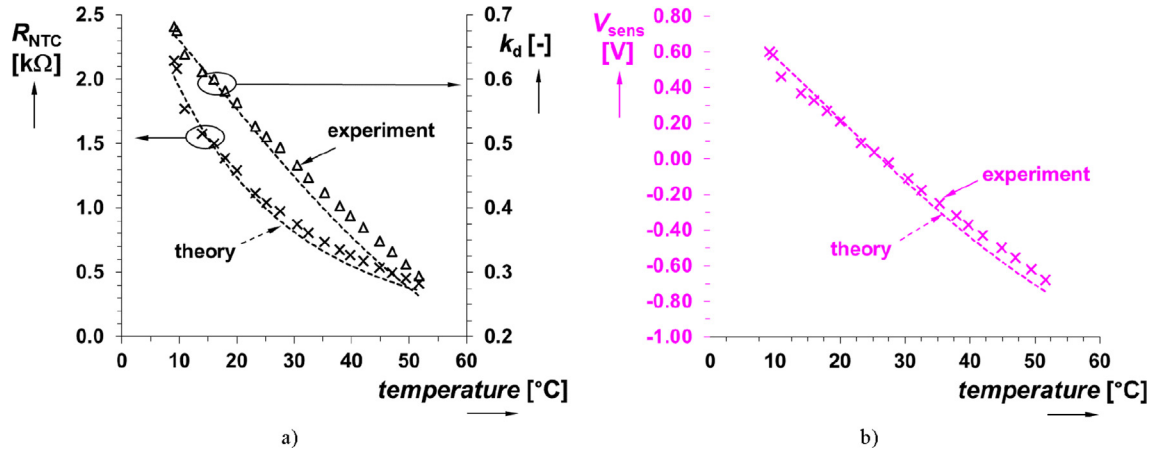

Fig. 16. Generation of V_{sens} based on resistive divider and thermistor: a) dependence of theoretical and measured resistance of R_{NTC} and transfer of divider on temperature, b) dependence of generated V_{sens} on temperature.

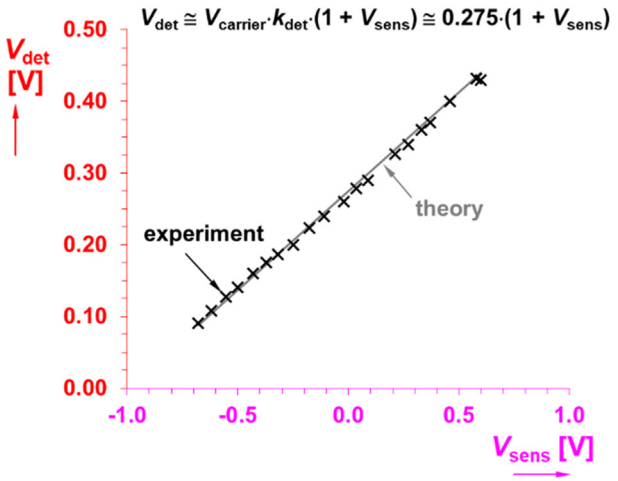

Fig. 17. Dependence of V_{det} on V_{sens}.

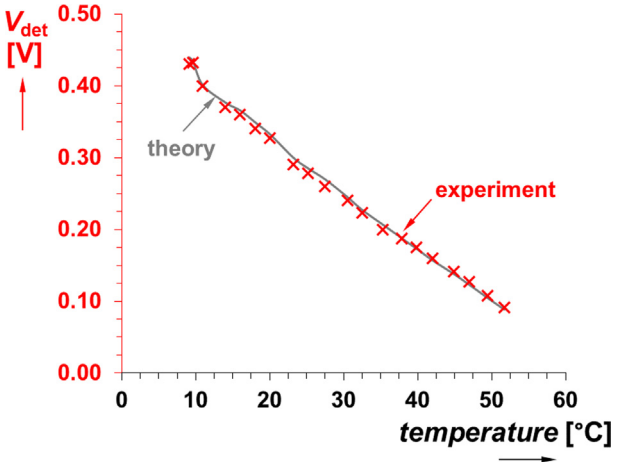

Fig. 18. Final relation between temperature and demodulated output voltage V_{det}.

approximate constant 0.275. The final relation between temperature and demodulated (detected) output voltage V_{det} (see Fig. 18) is result from (7), from the knowledge of k_{det} and $V_{carrier}$ and from experimental (decisive trace in comparison with inaccurate modeling by eq. (6)) dependence of V_{sens} on temperature (see Fig. 16 **(b)**).

We selected the presented application example of our system because methodology of temperature monitoring and measurement (in specific areas and conditions) represent substantial subjects of development typical for natural areas (plants, animals) [27] as well as for research relating with volcanic activity or space environments [28].

The following error graph (see Fig. 19) is provided to study errors through the system. Fig. 19 presents error of the detected DC output voltage V_{det} of the system calculated from variation of the measured V_{sens} voltage in dependence on temperature (i.e. theoretical trace in Fig. 19 is calculated from experimental data in Fig. 16 **(b)** –characteristic of temperature sensor $V_{sens} = f(temp.)$). This dependence indicates low and acceptable relative error below 4.5% in target range from 10 °C up to 50 °C). Previous analyses confirm operationability of the system. The resulting overall power

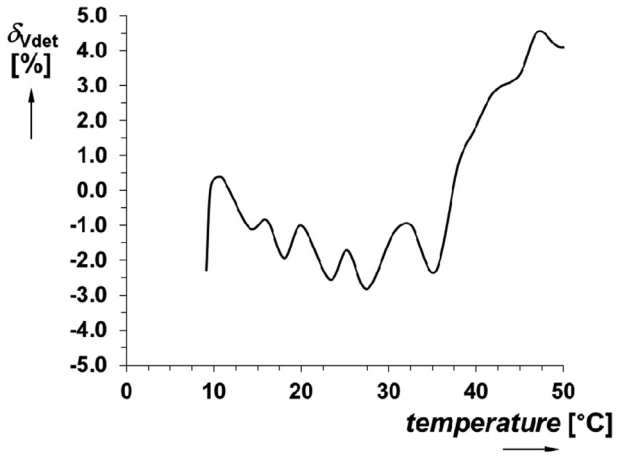

Fig. 19. Relative error observed in partial processing in dependence on temperature (errors between theoretical and measured V_{det}).

consumption (without arrangement of temperature sensor) reaches 59 mW.

We compared the performance of several solutions [29–34] regarding sensing features and accuracy of readout systems (sensor and supporting hardware). It must be noted that these solutions are not taking "wireless" transmission of the measured quantity (e.g. temperature) from closed environments into account. Results in Table 2 indicate that the active readouts (at the transmitter side), using temperature dependent elements of the resistive character, generating a DC voltage or data output, have errors in high units of % (it means several degrees when a very wide range of temperature is used [29,34]). Despite of this error, these solutions can be used sufficiently in specific cases. Many solutions use a quite extensive circuitry in some cases [29,31,34] or readouts (series modules) [30,32,33]. The calculated figure of merit (FOM) considers the declared measuring range of temperatures, complexity of readout and maximal absolute error. It seems that NTC thermistor-based approaches have very similar accuracy (including our sensor).

Application of temperature monitoring can be beneficially used for regulation purposes as it is indicated in [32,33] where the temperature of environment should be kept between 20 and 30 °C to keep good conditions for fish breeding, for example. In such a case, our simple analog solution may find beneficial advantages. Temperatures outside of the range 10 → 40 °C seem to be out of the good conditions for farming or growth. Our device indicates error below 2.8 °C with systematic offset of + 2 °C (that can be easily compensated) in this range. It must be noted that the inaccuracy in units of % is not critical for the intended applications. These applications and monitoring do not require highly accurate measurement of temperature because high tolerance of temperature variation (several units °C) is allowed. Fig. 20 shows the error of the sensor obtained in the observed temperature range (the measured temperature is calculated from the resistance value of R_{NTC} based on (6)). Note that difference between the expected (ideal) and the measured DC voltage at the output of the detector reaches 2–3%. The reason for this difference comes from inaccuracies of the estimated transfers in transmission and signal processing path. The main source of this error is the peak detector and pair of ferrite antennas.

Table 2
Brief comparison of sensors and readouts (hardware used at transmitting side) for temperature measurement used in recent works.

Reference	Wireless transmission from closed environment	Transmitted physical quantity for further processing outside of environment	Transmission distance (meters)	SW/digital processing not required	Number of passive/ active devices (transmission side)	Character of the system (area/topological complexity and processing)	Technology used for design	For low-cost applications	Sensor type	Tested temperature range [°C]	Absolute error [°C]	Transmission not influenced by environmental conditions (humidity, fog, vapor, etc.)	Figure of Merit (FOM)
[14]	Yes	modulated wave	0.02	No	>20	partially integrated/complex	350 nm CMOS fabricated	No	Thermistor (NTC)	+85→+135	N/A	Yes	–
[29]	No	DC voltage	N/A	N/A	12/1	discrete/simple	–	Yes	Thermistor (NTC)	−20→+80	−6→+7	N/A	1.1
[29]	No	DC voltage	N/A	N/A	18/4	discrete/simple	–	Yes	RTD	−20→+80	−0.3→ +0.3	N/A	15.2
[29]	No	DC voltage	N/A	N/A	7/1	discrete/simple	–	Yes	LM35	−20→+80	−0.3→ +0.7	N/A	17.9
[29]	No	DC voltage	N/A	N/A	–	discrete/simple	–	Yes	Thermocouple	−20→+80	+2→+6	N/A	–
[30]*	No	DC voltage	N/A	N/A	module	Complex	N/A	Yes	Thermistor (NTC)	5 → 90	−1.8→ +0.3	N/A	–
[31]	No	DC voltage	N/A	No	13 transistors + ADC	integrated/complex	65 nm CMOS fabricated	No	PTAT BJT	−20→+80	−0.4→ +0.2	N/A	17.9
[32]**	No	data	N/A	No	Modules, Arduino, +GSM/GPRS module	Complex	–	No	commercial sensor module	N/A	–	N/A	–
[33]	No	data	N/A	No	Modules, Arduino	Complex	–	No	commercial temperature probe	N/A	–	N/A	–
[34]	No	current (then data)	N/A	No	13/3 (amplification + ADC)	integrated/complex	180 nm TSMC fabricated	No	Fully integrated resistive bridge (thermal dependence of polyresistors)	−40→+85	−8→+5	N/A	0.97
This work (Fig. 1)	Yes	modulated wave	0.01	Yes	5/3	partially integrated/simple	350 nm CMOS fabricated	Yes	Thermistor (NTC)	10 → 50	−2.2→+3	Yes	1.7

*full Steinhart-Hart definition of nonlinear dependence of resistance on temperature used.
** wireless communication to mobile network (not considered as propagation from reservoir/aquarium to short distance).
NTC – thermistor with negative temperature dependent coefficient.
RTD – platinium resistance–temperature detector.
LM35 – commercial temperature silicon transducer.
PTAT BJT – change of base-emitter voltage proportional to absolute temperature at bipolar junction transistor.
FOM = temperature range / (number of active and passive devices · maximal absolute error).
ADC – analog to digital converter.
GSM/GPRS – Global System for Mobile network / General Packet Radio Service.

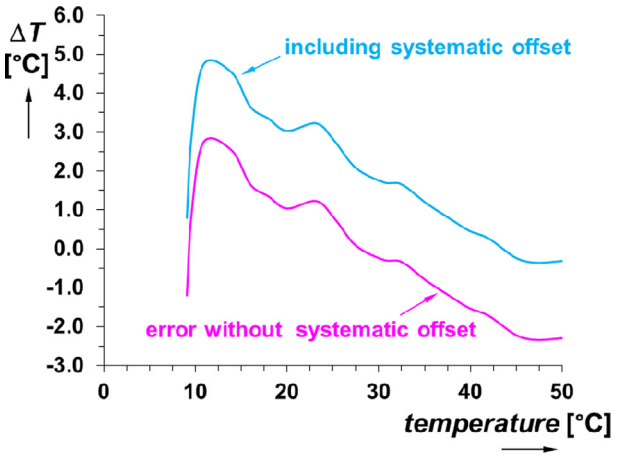

Fig. 20. Measurement: absolute error of the NTC sensor.

Conclusion

This paper brings a new concept of short range wireless communication system for transmission of RF signals from closed environments. The proposed system employs ferrite antennas and integrated active building parts fabricated in ON Semiconductor I3T25 0.35 μm CMOS process consuming 59 mW at 3.3 V (±1.65 V) power supply. The carrier frequency in medium-wave RF range (700 kHz) is used together with amplitude modulation technique (at the TX side) and amplifier (sufficient gain adjustable up to 9 dB) followed by an active detector at the RX side. The designed ferrite antennas (and their arrangement) used as wireless interface offer effective operation on short distance around 10 mm with insignificant attenuation of signal (approximately 7 dB). The useful low-frequency modulation signal has a bandwidth of 7.6 kHz that covers many applications. Tested situations shown transmission of sine and electrocardiogram signals in order to prove workability in the same frequency range with harmonic and non-harmonic signal. Despite low-voltage technology, voltage operational ranges are up to several hundreds of mV. The selected application example targets on the monitoring of temperature in isolated environments. When particular circuit with thermistor is added to produce the sensed signal, the whole system also offers temperature monitoring (from 10 °C up to 50 °C). The system itself has an ability to operate within error below 5% in the tested temperature range which is sufficient for specific application of environmental monitoring [32,33]. The difference between the expected (ideal) and the measured DC voltage at the output of the detector reaches 2–3%. The propagation of information about the sensed feature from the isolated area without significant loss of energy of signal (level) and without complicated amplification is fulfilled at this short distance of antennas. Therefore, the goals defined in the introductory part of this article are fulfilled. Specific applications of presented concept can be found in wide areas of laboratory testing and monitoring of environmental conditions when many agriculture [27] or environmental tests [28] are in progress.

Compliance with Ethics Requirements

This article does not contain any studies with human or animal subjects.

CRediT authorship contribution statement

Roman Sotner: Investigation, Writing – original draft, Visualization. **Jan Jerabek:** Writing – review & editing. **Ladislav Polak:** Visualization, Writing – review & editing. **Roman Prokop:** Investigation, Writing – review & editing. **Umut Engin Ayten:** Writing – review & editing. **Winai Jaikla:** Writing – review & editing.

Declaration of Competing Interest

The authors declare that they have no known competing financial interests or personal relationships that could have appeared to influence the work reported in this paper.

Acknowledgement

This work was supported by the Czech Science Foundation under Project 19-22248S.

References

[1] López-Larrea C. Sensing in nature. Switzerland: Springer Science+Business Media; 2012.
[2] Marchio E. The Art of Aquarium Keeping Communicates Science and Conservation. Frontiers Communication 2018;3:1–17. doi: https://doi.org/10.3389/fcomm.2018.00017.
[3] Zhang Z, Li Y, Mouthaan K, Lian Y. A Miniature Mode Reconfigurable Inductorless IR-UWB Transmitter-Receiver for Wireless Short-Range Communication and Vital-Sign Sensing. IEEE J Emer Sel Top Circ Sys 2018;2 (2):294–305. doi: https://doi.org/10.1109/JETCAS.2018.2799930.
[4] You X, Chen J, Zhong Y, Chen S, Yu C. Efficient Dimming Control with Time Domain Hybrid Modulation in Indoor Hybrid Visible Light/Infrared Communication Systems. In: *Proc. 24th Photonics in Switching and Computing Conf. (PSC)*, 2019, Fukuoka, Japan. p. 1–3. DOI: 10.23919/PS.2019.8817648
[5] Adiono T, Pradana A, Putra RWV, Cahyadi VA, Chung YH. Physical layer design with analog front end for bidirectional DCO-OFDM visible light communications. Optik 2017;138:103–18. doi: https://doi.org/10.1016/j.ijleo.2017.03.046.
[6] Vappangi S, Mani VV. Concurrent illumination and communication: A survey on Visible Light Communication. Phys Commun 2019;33:90–114. doi: https://doi.org/10.1016/j.phycom.2018.12.017.
[7] Sotner R, Jerabek J, Polak L, Petrzela J, Jaikla W, Tuntrakool S. Illuminance Sensing in Agriculture Applications Based on Infra-Red Short-Range Compact Transmitter Using 0.35 μm CMOS Active Device. IEEE Access 2020;8:18149–61. doi: https://doi.org/10.1109/ACCESS.2020.2966752.
[8] Barcik P, Hudcova L, Wilfert O. Influence of the Atmospheric Turbulence on the Laser Beam. In: Proc. 18th European Conf.e on Network and Optical Communications & 8th Conf. on Optical Cabling and Infrastructure (NOC-OC&I), 2013, Graz, Austria. p. 83–86, DOI: 10.1109/NOC-OCI.2013.6582872
[9] Barcik P, Hudcova L. Measurement of Spatial Coherence of Light Propagating in a Turbulent Atmosphere. Radioengineering 2013;22(1):341–5.
[10] Barcik P, Wilfert O, Dobesch A, Kolka Z, Hudcova L, Novak M, et al. Experimental measurement of the atmospheric turbulence effects and their influence on performance of fully photonic wireless communication receiver. Phys Commun 2018;31:212–7. doi: https://doi.org/10.1016/j.phycom.2018.05.003.
[11] Forster A. Radio Communications. Introduction to Wireless Sensor Networks, Hoboken, NJ, USA: Wiley; 2016.
[12] Straw RD. The ARRL Antenna Book: The Ultimate Reference for Amateur Radio Antennas, Transmission Lines and Propagation (Arrl Antenna Book). 21st edition. USA: American Radio Relay League; 2007.
[13] Leon-Gil J, Cortes-Loredo A, Fabian-Mijangos A, Martinez-Flores J, Tovar-Padilla M, Cardona-Castro M, et al. Medium and Short Wave RF Energy Harvester for Powering Wireless Sensor Networks. Sensors 2018;18(3):768. doi: https://doi.org/10.3390/s18030768.
[14] Li D et al. Wireless Sensing System-on-Chip for Near-Field Monitoring of Analog and Switch Quantities. IEEE Trans Ind Electron 2012;59(2):1288–99. doi: https://doi.org/10.1109/TIE.2011.2148676.
[15] Jingcheng L, Carr JL, Zhou CJ, Reyes MA, Noll JD. A Method for Estimating the Low Frequency Coupling Characteristics of a Ferrite-Cored Rod Antenna to a Long Conductor. Progress in Electromagnetics Research M 2018;75:193–203. doi: https://doi.org/10.2528/PIERM18081507.
[16] Seong YJ, Lee SS. A Study on Precise Positioning for an Electric Vehicle Wireless Power Transfer System Using a Ferrite Antenna. Electronics 2020;9(8):1–27. doi: https://doi.org/10.3390/electronics9081289.
[17] Debnath S. Network coverage using MI waves for underwater wireless sensor network in shadowing environment. IET Microw. Antennas & Propag. 2021; 15 (9): 1035–1041. DOI: 0.1049/mia2.12113
[18] Sotner R, Jerabek J, Polak L, Prokop R, Kledrowetz V. Integrated Building Cells for a Simple Modular Design of Electronic Circuits with Reduced External Complexity: Performance, Active Element Assembly, and an Application Example. Electronics 2019; 8(5): 1–26. DOI: 0.3390/electronics8050568
[19] Biolek D, Senani R, Biolkova V, Kolka Z. Active elements for analog signal processing: Classification. Review and New Proposals. Radioengineering 2008;17(4):15–32.

[20] Senani R, Bhaskar DR, Singh AK. Current Conveyors. Cham: Springer International Publishing; 2015.
[21] ON Semiconductor, I3T Process Technology [accessible on: http://www.europractice-ic.com/technologies_AMIS_tech.php]
[23] Stavroulakis P. Interference Analysis and Reduction for Wireless Systems. UK: Artech House; 2003.
[22] Vishay, BAT42, BAT 43 Small Signal Schottky Diode (datasheet) [accessible on: https://www.vishay.com/docs/85660/bat42.pdf]
[24] EPCOS, B57045K NTC thermistor for temperature measurement (datasheet) [accessible on: https://www.tme.eu/Document/df738e1694624b65da1709a66f31062a/B57045.pdf]
[25] Childs PRN, Greenwood JR, Long CA. Review of temperature measurement. Rev Sci Instrum 2000;71(8):2959–78. doi: https://doi.org/10.1063/1.1305516.
[26] Aleksic O, Nikolic P. Recent advances in NTC thick film thermistor properties and applications. Facta Universitatis-Series: Electronics and Energetics 2017;30(3):267–84. doi: https://doi.org/10.2298/FUEE1703267A.
[27] Xiao Q, Bai X, Zhang C, He Y. Advanced high-throughput plant phenotyping techniques for genome-wide association studies: A review. J Adv Res 2022;35:215–30.
[28] Biktash L. Long-term global temperature variations under total solar irradiance, cosmic rays, and volcanic activity. J Adv Res 2017;8(4):329–32. doi: https://doi.org/10.1016/j.jare.2017.03.002.
[29] Trancă DC, Rosner D, Tătăroiu R, Stegaru SC, Surpățeanu A, Peišić M. Precision and linearity of analog temperature sensors for industrial IoT devices. 2018 17th RoEduNet Conference: Networking in Education and Research (RoEduNet). p. 1–6. doi: https://doi.org/10.1109/ROEDUNET.2018.8514122.
[30] Laktionov I, Lebediev V, Vovna O, Zolotarova O, Sukach S. Results of Researches of Metrological Characteristics of Analog Temperature Sensors. IEEE Int Conf Modern Electrical Energy Systems (MEES) 2019;2019:478–81. doi: https://doi.org/10.1109/MEES.2019.8896378.
[31] Caselli M, Ronchi M, Boni A. An Integrated Low Power Temperature Sensor for Food Monitoring Applications. IEEE Int Symposium Circuits Systems (ISCAS) 2021;2021:1–4. doi: https://doi.org/10.1109/ISCAS51556.2021.9401361.
[32] Siregar B, Rachman F, Efendi S, Sulindawaty. Monitoring the Value of Water Quality and Condition Parameters Using the Open Sensor Aquarium. J Phys Conf Ser 2019;1255(1):012036. doi: https://doi.org/10.1088/1742-6596/1255/1/012036.
[33] Salim TI, Haiyunnisa T, Alam HS. Design and implementation of water quality monitoring for eel fish aquaculture. Int Symposium Electronics Smart Devices (ISESD) 2016;2016:208–13. doi: https://doi.org/10.1109/ISESD.2016.7886720.
[34] Pan S, Jiang H, Makinwa KAA. A CMOS temperature sensor with a 49fJK2 resolution FoM. Symposium VLSI Circuits 2017;2017:C82–3. doi: https://doi.org/10.23919/VLSIC.2017.8008557.